ChemPubSoc Europe

DOI: 10.1002/slct.201701693

Chemistry SELECT Full Papers

Catalysis

Immobilizing Multifunctional Fe_2O_3-SnO_2 Nanoparticles to Carbon Nanospheres: An Extremely Active and Selective Catalyst for Hydrogen Transfer Reaction

Li Qi,[a] Yunong Li,[a] Lei Liu,[a] Junjie Zhou,[a] Yongjian Ai,[a, b] Zhike Tang,[a] Jingting Wang,[a] Hongjie Bao,[a] Cheng Zhang,[a] Qionglin Liang,[b] Hongbin Sun,*[a] and Dun Niu*[a]

In this paper, we have developed a new branch of multifunctional iron tin oxide composite as an efficient catalyst for the reduction of the nitroarenes. The iron-tin bimetallic oxide nanoparticles anchored on the carrier of carbon nanospheres synthesized by hydrothermal carbonization (HTC) were the active sites. And in the presence of the multi-component catalyst C@Fe2O3-SnO2, the nitroaromatics were quantitatively converted into aromatic amines with the hydrogen source of hydrazine hydrate. The synergy interaction between the two kinds of metallic oxides provided a certain enhancement for the catalytic activity of iron based catalyst. Moreover, these nanocatalysts could be collected through magnetic separation, and recycled for 10 times without any loss of catalytic activity. These results showed that the catalyst system possessed the superiority of wide application scope, safety, high efficiency and good chemoselectivity.

Introduction

Aromatic amines are extremely important chemical intermediates for their widespread applications in the herbicides, insecticides, synthetic dye, pharmaceuticals etc. Hence, the synthesis of aromatic amine has attracted considerable attention both in industry and laboratory.[1] In this context, the reduction of aromatic nitro compounds to produce aromatic amines is more significant. Traditional process via iron powder and hydrochloric acid could effectively restore a nitro into amino,[2] but this method has caused environmental pollution.[3] Catalytic hydrogenation can serve as a replacement of the iron powder reduction for its clean procedure and high yield,[4] but it is subjected to the limitation of its equipment investment and high operating costs. Therefore, people are constantly exploring more environmentally and economically advantageous methods.[5] Notably, the reduction of nitro compounds with hydrazine hydrate as the reducing agent is a simple, economical and environmentally friendly method,[6] because the by-products are only eco-friendly nitrogen and water, and less safety concern is required for neither complex operation nor expensive equipment.

However, the neat hydrazine mediated reduction of nitro to amino requires high pressure and long reaction time,[7] so a variety of catalysts have been designed to perform the reactions in mild and efficient way. It is well known that some precious metal catalysts such as Au,[8] Ru,[9] Pd,[10] and Rh[11] have shown good effect in this transformation, but suffering from their expensiveness and scarcity, the application range was not wide enough. In this context, the iron based catalysts have shown great advantages for their low cost and non-toxic nature.[12] Since Lauwiner, Benz and co-workers reported a series of systematic research work on the iron oxide catalyzed the hydrazine-mediated reduction of nitroarenes in 1998~1999,[13] various iron oxide based catalysts have been applied to improve the catalytic activity and selectivity.[14] However, the mono-component iron oxide catalyst lacks stability and reusability, more efforts have been developed to improve its efficiency, such as the immobilization of hydrazine and the doping of the iron oxide.[15] Bimetallic oxide is another promising way,[16] because the combination of another oxide to iron oxide can significantly improve the performance via adjusting its electrical properties,[17] while iron oxide is usually considered as a narrow band gap n-type semiconductor (e.g. 2.2 eV for Fe_2O_3).

There are evidences that mixing the two oxides can really improve the performance as catalyst. SnO_2 is considered as the promising modifier, because it is a direct band gap n-type semiconductor (~3.8 eV) and has attracted much attention on account of its extensive application in Li-ion battery storage,[18] gas sensors,[19] photoelectrochemical material[20] and photo catalysis.[21] Moreover, the tin iron oxide composites are the well-known multifunctional materials, and they have been widely used in various fields, such as Li-ion battery storage, super capacitor, gas sensor and photocatalysts.[22] It has been demonstrated that the synergistic effect between Fe_2O_3/SnO_2

[a] L. Qi, Y. Li, L. Liu, J. Zhou, Y. Ai, Z. Tang, J. Wang, H. Bao, C. Zhang, Dr. H. Sun, Dr. D. Niu
Department of Chemistry
Northeastern University
Shenyang 110819, People's Republic of China
E-mail: sunhb@mail.neu.edu.cn
niudun666@hotmail.com
[b] Y. Ai, Dr. Q. Liang
Department of Chemistry
Tsinghua University
Beijing 100084, People's Republic of China

Supporting information for this article is available on the WWW under https://doi.org/10.1002/slct.201701693

composites could greatly enlarge their application range, and the composite possess higher sensitivity and better electrochemical activity compared to the single component of SnO_2 or Fe_2O_3.

However, the supporter-free composite materials are usually less active catalysts, and a carbon carrier has been demonstrated effective for the reduction of nitro compounds.[23] In our visual sense, carbon nanospheres stand out from multitudinous carbonaceous nanomaterials (nanofibers, nanotubes, nanospheres, graphene, etc.) owing to the following reasons: a) easiness of preparation;[24] b) controllable morphologies;[25] c) large specific surface area;[26] d) microporosities or mesoporosities;[27] e) highly reactive activities.[28] Compositing nanoparticles with carbon nanospheres can effectively improve the uniformity,[29] dispersity,[30] stability[31] and sensitivity[32] of the target material. In addition, what impresses us more is its good electrical conductivity,[33] which is beneficial to the reduction of nitro compound. So the carbon nanospheres are elected as the promising candidate of catalyst supporter.

Inspired by the bimetallic oxide catalysts and according to the designation above, we developed the active Fe_2O_3-SnO_2 nanoparticles germinated in carbon nanospheres as the highly efficient and selective catalysts for the transfer hydrogenation of nitroaromatics. We synthesized the carbon nanospheres by hydrothermal carbonization (HTC) processing[34] and used them as the carrier. The iron-tin oxides composite nanoparticles were tightly bound to the carrier as the active substance (Scheme 1).

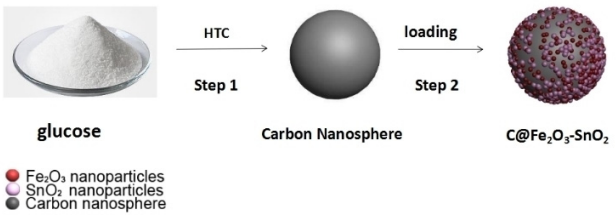

Scheme 1. Brief schematic illustration of the synthesis of the C@Fe_2O_3-SnO_2.

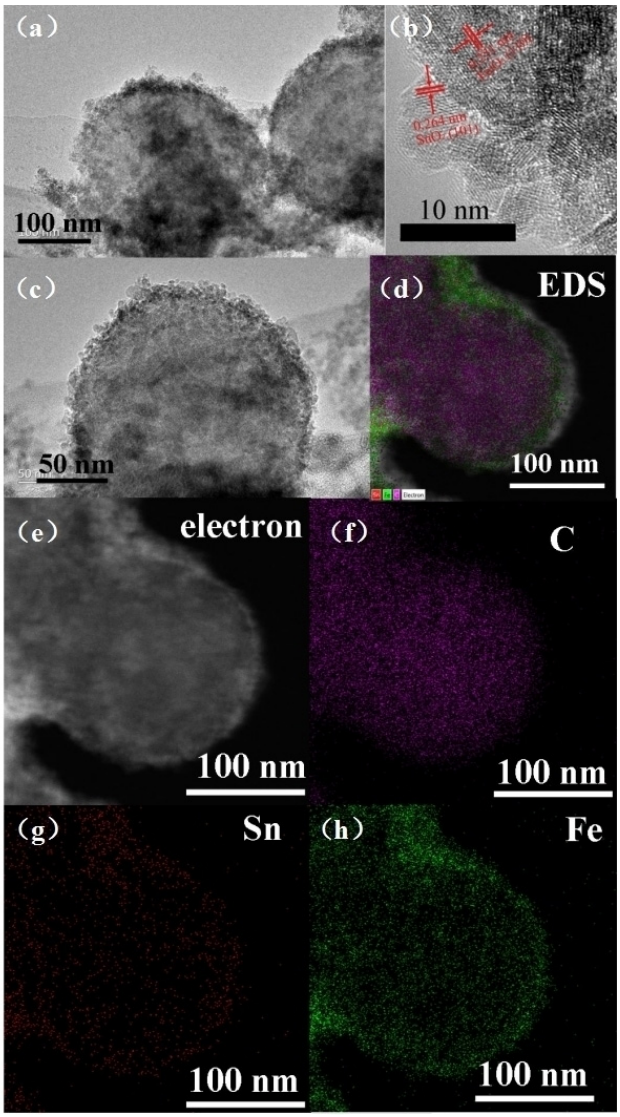

Figure 1. (a, b and c) HRTEM images of C@Fe2O3-SnO_2;(d, f, g, and h) EDS elemental mappings of the spherical catalyst;(e)corresponding electron image.

To our delight, the developed catalyst exhibited expected excellent catalytic activity. This is a new branch for the well-known multifunctional material Fe_2O_3/SnO_2.

Results and Discussion

Characterization of the identified catalyst

The ultimate catalysts were systematically characterized by transmission electron microscopy (TEM), X-ray diffraction (XRD), FTIR analysis, X-ray photoelectron spectroscopy (XPS), Brunauer-Emmett-Teller(BET) and Vibrating Sample Magnetometer (VSM).

For C@Fe_2O_3-SnO_2 catalyst, as shown in Figure 1, Fe_2O_3 and SnO_2 nanoparticles are successfully immobilized on carbon nanospheres. The homemade carbon nanospheres are in the size of about 200 nm, and the active material Fe_2O_3 and SnO_2 nanoparticles are evenly dispersed with an average particle size of about 5~6 nm. In addition, the EDS analysis (Figure 1d, f, g, h) reveals that the composition of hierarchical composites consisted of C, Sn and Fe elements. It can be clearly demonstrated that the two elements are firmly wrapped on the carbon nanosphere substrate from Figure 1d. Moreover, through the HRTEM (Figure 1b) we can clearly recognize the lattice stripes, which reveal the characteristic facet of SnO_2 and α-Fe_2O_3. And according to these lattice spacing and grain size, we can estimate that the number of Fe surface sites is 7.08×10^{-3} mmol compared to the theoretical value of 17.6×10^{-3} mmol (calculation details can be found in the supporting informations).

As shown in Figure 2(a), the 2θ range from 20° to 90° was scanned and all peaks (C@Fe_2O_3-SnO_2) matched the standard

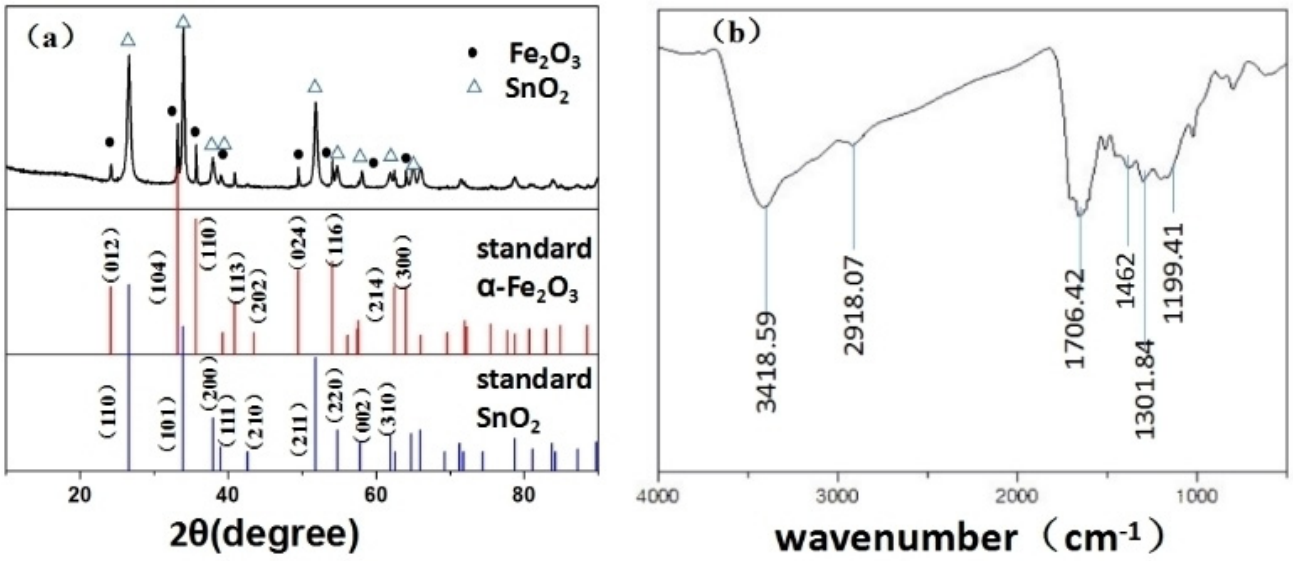

Figure 2. (a) XRD patterns of C@Fe_2O_3-SnO_2; (b) FTIR Spectrum of the carbon nanospheres.

data for α-Fe_2O_3 and SnO_2. The diffraction peaks at 2θ = 27.1°, 33.6°, 38.3°, 52.8°, 54.4° and 62.1° respectively, can be attributed to the tetragonal SnO_2 [110], [101], [200], [211], [220] and [310] crystal face. And the diffraction peaks at 22.8°, 31.6°, 36.4°, 39.9° and 52.7° were attributed to [002], [104], [110], [024] and [116] facets of hexagonal structure Fe_2O_3. In addition, the diffraction peaks thickly dotted between 55° to 62° illustrated that SnO_2 and Fe_2O_3 perfectly compounded. These coherent peaks flock indicate the synergy of SnO_2 and Fe_2O_3, which brings the outstanding efficiency for the catalytic reduction of nitro groups.

In order to analyze the feasibility of the carbon carriers to support metal oxides, the Fourier Transform infrared spectroscopy (FTIR) has been analyzed (Figure 2(b)). The characteristic peak at 3418 cm^{-1} was due to the presence of O–H bond, while the band around 2918 cm^{-1} was assigned to the stretching vibrations of the -CH_2 group, and the peak at 1462 cm^{-1} was assigned to be the bending vibration of CH. The broad peak centered around 1706 cm^{-1} exhibited an envelope of stretching vibrations for C=O. The peaks at 3418, 1706 and 1301 cm^{-1} evidenced the existence of -COOH, and 3418 and 1199 cm^{-1} indicated the -OH group. The FTIR spectra indicated that there were a lot of -OH and -COOH groups on the surface of the carbon nanospheres, which favored the demand of grafting the metal oxide active layer on the surface.

The electronic states of metal elements in the homemade C@Fe_2O_3-SnO_2 were further examined by XPS. The determination of binding energy was based on the C 1s at 284.8 eV with an experimental error of ±0.4 eV. The Fe 2p spectrum of the self-made C@Fe_2O_3-SnO_2 was shown in Figure 3(b) while the Sn 3d spectrum was shown in Figure 3(c). From the survey spectrum Figure 3(a), there was almost no difference between the as-prepared catalyst and the 10 cycles used one. And as shown in Figure 3(b), the presence of C@Fe_2O_3-SnO_2 could be further determined by the Fe 2p XPS peaks at 715.6 and 724.1 eV, which attributed to Fe^{3+} $2P_{3/2}$ and Fe^{3+} $2P_{1/2}$, respectively. The binding energy values for the Fe^{2+} and Fe^{3+} peaks were in agreement with the reported data of Fe 2P binding energy values. Figure 3(b) and (c) consist of component peaks at 716.8, 486.4 and 494.8 eV, which could be ascribed to Sn $3P_{3/2}$, Sn $3d_{5/2}$, and Sn $3d_{3/2}$ groups, respectively. Clearly, the XPS spectra provided important information of the oxidation state of atom within C@Fe_2O_3-SnO_2. The binding energy values for the Sn^{4+} peaks were in agreement with the NIST database of Sn 3d binding energy values in SnO_2, which indicated that there was no structural change of the SnO_2 nanoparticles before and after the reaction.

Figure 4(a) presents the typical N_2 adsorption-desorption isotherm of the as-prepared catalyst C@Fe_2O_3-SnO_2 sample. It exhibits prominent characteristics of type-IV isotherms, and the H2 hysteresis loop (0.4-0.8) indicates the typical mesoporous structure. With the increase of P/P0, the amount of adsorption increased gently in the low pressure range (0 ~ 0.5), this can be deduced as the N_2 molecules were adsorbed on the inner surface. In the range of P/P0 = 0.5 ~ 0.8, the adsorption capacity has a sharp increase, this may because of the capillary condensation, and the sharp increase reflects the pore size is uniform. Moreover, the pore size distribution is given in Figure 4b. As can be seen, the C@Fe_2O_3-SnO_2 shows a relatively narrow pore distribution mainly in the mesoporous region of 40–80 nm (average 48.78 nm). In addition, the BET surface area of the C@Fe_2O_3-SnO_2 sample was measured to be 134.5 m^2 g^{-1} which can lead to a better mass transport performance.

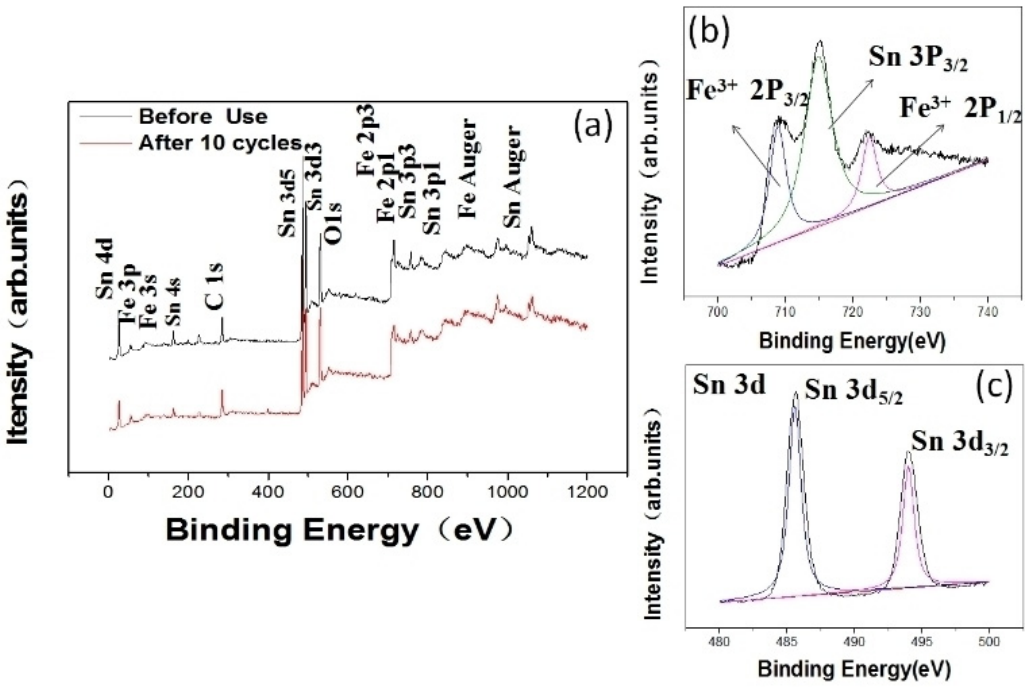

Figure 3. (a) XPS of as-prepared catalyst C@Fe_2O_3-SnO_2 and after 10 cycles; (b) XPS Fe 2P spectra; (c) XPS Sn 3d spectra.

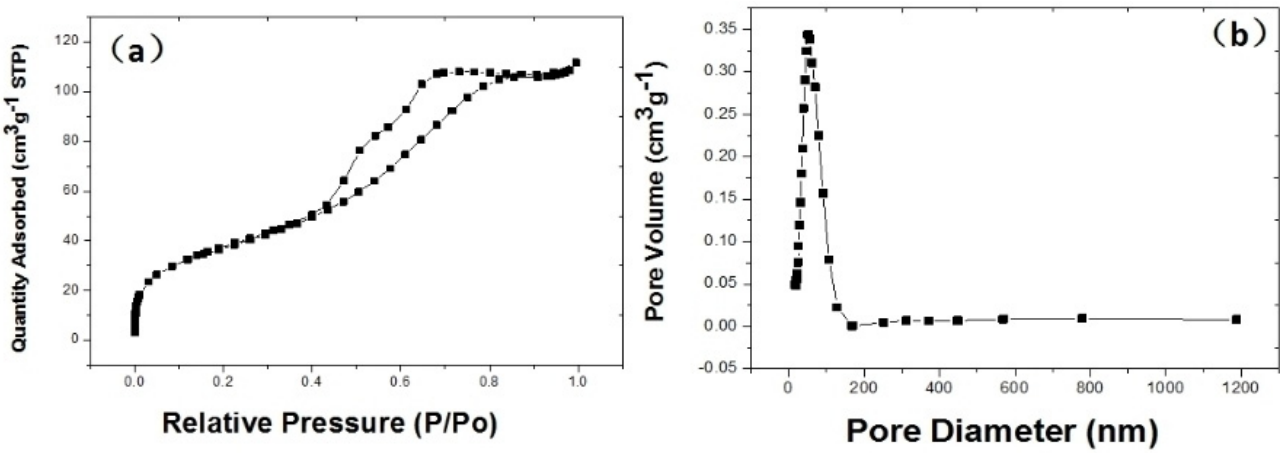

Figure 4. (a) N_2 adsorption-desorption isotherm; (b) Pore volume and pore diameter.

The optimization of catalysts and the conditions of reduction

In order to evaluate different catalysts and determine the best solvent for the $N_2H_4{\cdot}H_2O$ mediated reduction, the optimization experiments have been carried out with the model reaction of 4-nitrophenol into 4-aminophenol as shown in Table 1[a] (The exploration of temperature for the reaction system was shown in supporting information Table S1).

A series of synthesized catalysts were tested in the reduction of p-nitrophenol in a sealed tube to check the catalytic performances and choose the most active catalyst (Table 1). It showed that in the absence of catalyst, no product can be detected in this system. Carbon could play a catalytic role as similar to the known reports, but the effect was minimal (Table 1, entries 1~2). For individual metal oxide, the catalytic effect of iron oxide (especially Fe_2O_3, whose effect was even better than Fe_3O_4) was slightly better than tin oxide, but after the combination of the bimetallic oxides, the effect was greatly enhanced (Table 1, entries 3~6). If we used the carbon nanospheres as the carrier to support metal oxide, the effect would be much better (Table 1, entries 7~9). This was because the supporter-free composite materials were usually unstable, so the effect was not as effective as carbon carrier catalysts. As evidenced in Table 1, the C@Fe_2O_3-SnO_2=2:1 nanocatalyst (entry 11) exhibited the best catalytic activity among other proportional investigated compositions (entries 10~13).

After determinating the catalyst, we examined the optimum solvents for the reaction system. Changing the solvent had an obvious effect on the product yield (Table 1, entries 11, 14~17).

Table 1. The optimization of C@Fe_2O_3-SnO_2 catalyzed reduction of 4-nitrophenol [a]

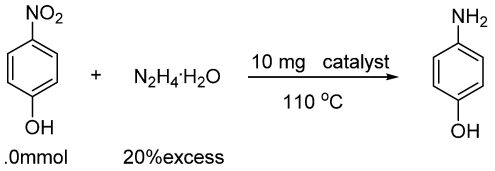

1.0mmol 20%excess

Entry	Catalyst	Solvent	Yield(%)[b]
1	-	Methanol	0
2	C	Methanol	4.61
3	Fe_2O_3	Methanol	14.57
4	Fe_3O_4	Methanol	12.16
5	SnO_2	Methanol	3.18
6	Fe_2O_3-SnO_2	Methanol	32.16
7	C@Fe_3O_4	Methanol	47.63
8	C@Fe_2O_3	Methanol	54.95
9	C@SnO_2	Methanol	24.68
10	C@Fe_2O_3-SnO_2=1:1	Methanol	79.24[c]
11	C@Fe_2O_3-SnO_2=2:1	Methanol	100[c]
12	C@Fe_2O_3-SnO_2=5:1	Methanol	70.45[c]
13	C@Fe_2O_3-SnO_2=10:1	Methanol	92.52[c]
14	C@Fe_2O_3-SnO_2=2:1	Water	41.75[c]
15	C@Fe_2O_3-SnO_2=2:1	Ethanol	98.57[c]
16	C@Fe_2O_3-SnO_2=2:1	Isopropanol	95.31[c]
17	C@Fe_2O_3-SnO_2=2:1	Ethylene glycol /methanol (1:1)[d]	74.57[c]

[a] All the reactions were carried out under the general conditions: 4-nitrophenol (1 mmol), 20% excess hydrazine hydrate (1.8 mmol), solvent (2 mL), temperature (110°C), catalyst (10 mg). [b] Yields were determined by HPLC. [c] Based on the mass ratio of $FeCl_3·6H_2O$ and $SnCl_4·5H_2O$. [d] When the solvent was single ethylene glycol, we found there was undissolved 4-nitrophenol, so we utilized the mixed solvent of ethylene glycol /methanol (1:1), which can fully dissolve 4-nitrophenol.

Under the same temperature response for an hour, we could summarize that excellent yields were obtained in methanol, ethanol and isopropyl alcohol. In contrast, when we used ethylene glycol especially water as the solvent, the yield was unacceptable. As is known to all, solvent effect, that is polarity effect, is the answer of the question. According to the polarity order (water > ethylene glycol > methanol > ethanol > isopropyl alcohol), we speculated that this reaction system is not suitable for strong polar solvent environment. Thus, we chose methyl alcohol as the optimal solvent

The substrate scope exploration

With the most effective catalyst and optimized reaction conditions in hand, various nitroarenes were taken into account to inspect our catalyst. The results are summarized in Table 2.

On the whole, the reactions were relatively completed and all substrates afforded the target product in excellent yields. This confirmed the superiority of the catalyst, whose catalytic activity was contributed from the synergy of the semiconductor metal oxides. It's well known that dehalogenation is always accompanied by the process of hydrogenation of nitro. In order to validate the catalytic selectivity of C@Fe_2O_3-SnO_2, we tested seven substrates containing halogen. To our delight, both simple substrates such as *p*-chloronitrobenzene and *o*-chloronitrobenzene (Table 2, entries 1, 3) and complex compounds such as 4-chloro-2-nitrophenol and 4-(4-Chlorophenoxy) nitrobenzene (entries 12, 16) showed good selectivity without any dehalogenation phenomenon. A particularly worth mentioning substrate was 2, 6-dichloro-4-nitrophenol that overcame space steric hindrance, it was smoothly reduced to 2, 6-dichloro-4-aminophenol (entry 20). We also tested substrates with bromide and fluoride, and the results showed that the chloronitroarene was the most stable one among the halo-substrates, because the 4-fluoro-nitrobenzene gave 4% defluorinated product (un-substituted aniline) and the 3-bromo-nitrobenzene gave trace (< 0.4%) debrominated product (entries 4, 5). What's more, this catalyst system was also chemoselective for other functionalized nitroarenes, including the derivatives that contained alcohol, acid, ester group, ether, amide and amino group. These nitroarenes completely transformed into the corresponding anilines and we detected no decomposition of other functional groups (entries 6~11, 13, 21). Prominently, some substrates bearing heterocyclic ring widened the scope of our catalytic system. They were smoothly converted into the corresponding anilines with satisfactory yields, while the heterocyclic rings remained intact (entries 14~15, 18~19). Most important of all, we had not detected any azoxy, azo and hydrazo compounds that usually generated as the by-products in the reduction of nitroarenes.

Everything according to our design, there are two unparalleled advantages of our catalytic system. First of all, the synergistic effect between the two different metallic oxides offered extraordinary activity, thus the nanocomposite shows better performance than the individual components. Excellent electrochemical performance is one of the best representatives (the good capacitance characteristics are shown in Figure S2 (a), (b), Supporting Information). The core-shell structural features are another important point. The nanoscale spherical structure of the carbon-carrier increases the contact between the active sites and the reactants, and the surface-distributed outer active layer also facilitates the entry of the reaction solution, which greatly improves the reaction rate. Also, the magnetic property makes the catalyst can be separated by an

Table 2. Substrate scope of the catalytic reaction over C @ Fe_2O_3-SnO_2 under optimized conditions [a].

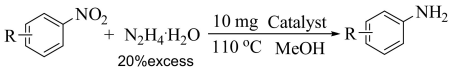

Entry	Substrate	Time/min	Product	Yield(%)[b]	TOF(h^{-1})
1	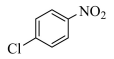	40	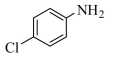	>99	212
2	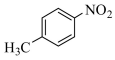	40	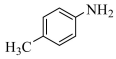	>99	212
3		40		>99	212
4	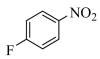	60	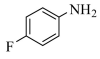	96	141
5	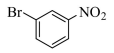	40	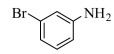	>99	212
6	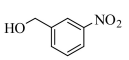	40	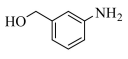	>99	212
7	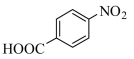	60	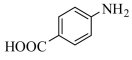	>99	141
8	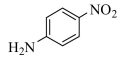	40	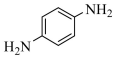	>99	212
9	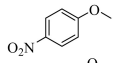	40	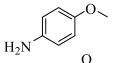	>99	212
10	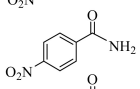	40	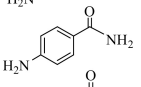	>99	212
11	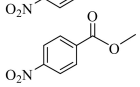	60	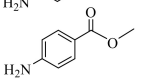	>99	141
12	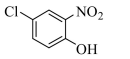	60	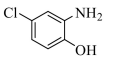	>99	141
13	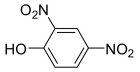	60	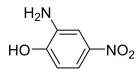	93	141
14	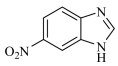	60	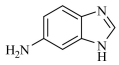	>99	141
15	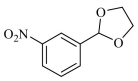	60	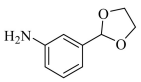	>99	141
16	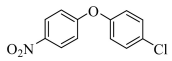	40	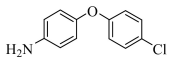	>99	212
17	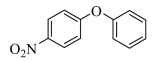	40	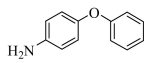	>99	212
18	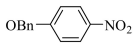	60	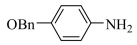	>99	141
19	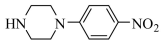	60	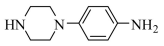	>99	141
20	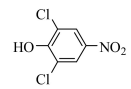	60		>99	141
21		90		>99	94

[a] all the reactions were carried out with 1 mmol nitroarenes, 1.8 eq. hydrazine hydrate and 10 mg catalyst in 2 mL methanol solvent; [b] Determined as HPLC peak area percentage.

external magnet, in spite of the magnetism is not very strong (Figure 5a). The combined advantagement provides certain new inspiring and learning for the catalyst design. Another advantage of our catalyst is its reusability. The recyclability of our catalyst was investigated with the model reaction of converting 4-nitrophenol to 4-aminophenol at the optimized reaction conditions. The catalyst could be collected via magnetic separation and washed with methanol and ultimately dried for next reaction cycle. The recycling test showed that the catalyst was robust and could be reused up to 10 times within negligible loss of the catalytic activity (Figure 5b).

Mechanism

According to the reported literatures and the experimental results,[35] an approbatory reaction mechanism has been proposed as shown in Scheme 2. In this reaction process, first

Scheme 2. Schematic representation of hydrogenation using C@Fe_2O_3-SnO_2.

of all, dissociative nitroaromatics and N_2H_4·H_2O under the effect of diffusion are adsorbed on the surface of the catalyst, then the N_2H_4·H_2O orders to lose electrons and generates N_2 and active H species. The active layer undergoes rapid electron transfer and hydrogen exchange to complete full reaction. It has been reported that the Fe^{2+}/Fe^{3+} REDOX cycle in the hybrid catalyst is the root of the catalytic activity,[36] and the believable effect of the SnO_2 is that it accelerates the oxidation of Fe^{2+} to Fe^{3+}, thus enhances the Fe^{2+}/Fe^{3+} REDOX cycle.[37] The specific step is generating active H species and the transferring electron to the adsorbed nitroaromatics, and then the nitro compound is gradually reduced and finally to aniline. The overall mechanisms have been identified as : Ar-NO_2→Ar-NO→Ar-NHOH→Ar-NH_2. In terms of our catalyst, the existence of carbon sphere and tin oxide increases the conductivity of the catalyst particle, and this leads to a more efficient electron transportation.

Conclusions

In conclusion, a new branch of the multifunctional material Fe_2O_3-SnO_2 was developed. It is a highly efficient, easy-to-handle catalyst with good chemoselectivity for the hydrazine hydrate mediated reduction of the nitroarenes into aromatic amines. The iron-based catalyst was remarkably enhanced by doping

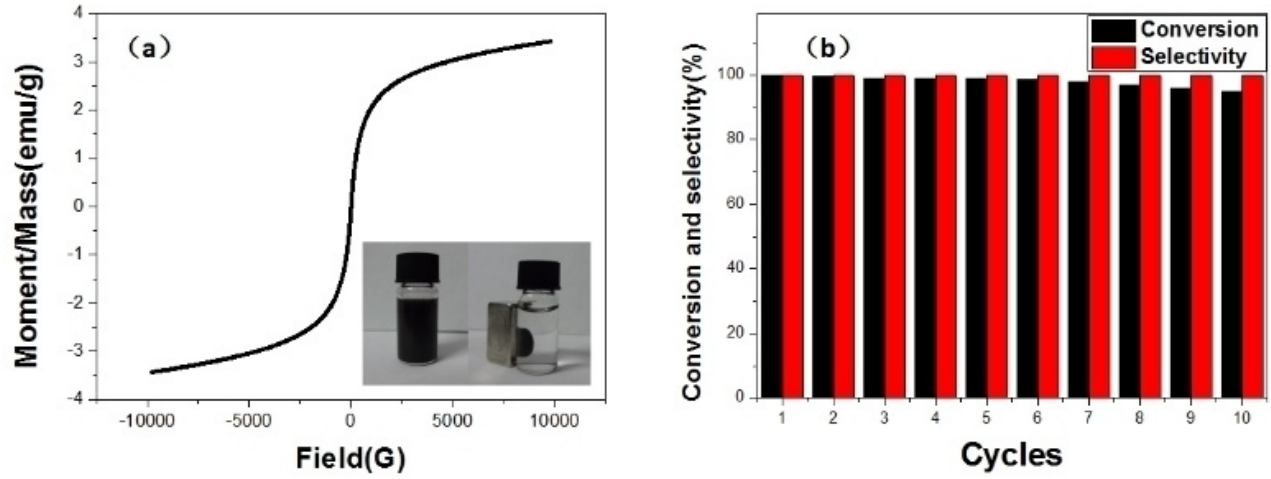

Figure 5. (a) Magnetization curve(insert was the rendering of magnet adsorption); (b) Recyclability of the catalyst.

semiconductor metal oxide SnO_2, and the carbon sphere supporter further improved its catalytic activity. Employing the iron tin bimetallic oxide catalyst C@Fe_2O_3-SnO_2, complete conversions were achieved with a series of nitroarenes as substrates within short time. Remarkably, the magnetically separable catalyst could be reused for about ten cycles without any loss of catalytic activity. It was worth mentioning that digging the new application of well-studied multifunctional material is a promising idea to develop the more practical and efficient catalyst, as well as to illustrate the catalytic mechanism with the known effect.

Acknowledgements

This work was financially supported by National Natural Science Foundation of China (21235004, 21175080) and the Ministry of Science and Technology (2013ZX09507005).

Conflict of Interest

The authors declare no conflict of interest.

Keywords: Anilines · Carbon Nanospheres · Catalytic Reduction · Iron-Tin Oxide · Nitroarenes

[1] a) R. S. Downing, P. J. Kunkeler, H. VanBekkum, *Catal. Today* **1997**, *37*, 121–136; b) A. M. Tafesh, J. Weiguny, *Chem. Rev.* **1996**, *96*, 2035–2052; c) Z. Dong, X. Le, C. Dong, W. Zhang, X. Li, J. Ma, *Appl. Catal., B* **2015**, *162*, 372–380; d) P. Zhou, Z. Zhang, L. Jiang, C. Yu, K. Lv, J. Sun, S. Wang, *Appl. Catal., B* **2017**, *210*, 522–532.

[2] Y. G. Liu, Y. S. Lu, M. Prashad, J. Repic, T. J. Blacklock, *Adv. Synth. Catal.* **2005**, *347*, 217–219.

[3] R. Dey, N. Mukherjee, S. Ahammed, B. C. Ranu, *Chem. Commun.* **2012**, *48*, 7982–7984.

[4] R. V. Jagadeesh, A.-E. Surkus, H. Junge, M.-M. Pohl, J. Radnik, J. Rabeah, H. Huan, V. Schuenemann, A. Brueckner, M. Beller, *Science* **2013**, *342*, 1073–1076.

[5] a) S. Fountoulaki, V. Daikopoulou, P. L. Gkizis, I. Tamiolakis, G. S. Armatas, I. N. Lykakis, *ACS Catal.* **2014**, *4*, 3504–3511; b) M. B. Gawande, A. K. Rathi, J. Tucek, K. Safarova, N. Bundaleski, O. M. N. D. Teodoro, L. Kvitek, R. S. Varma, R. Zboril, *Green Chem.* **2014**, *16*, 4137–4143; c) R. Sedghi, M. M. Heravi, S. Asadi, N. Nazari, M. R. Nabid, *Curr. Org. Chem.* **2016**, *20*, 696–734; d) H. Goksu, S. F. Ho, O. Metin, K. Korkmaz, A. M. Garcia, M. S. Gultekin, S. Sun, *ACS Catal.* **2014**, *4*, 1777–1782; e) P. Zhou, Z. Zhang, *ChemSuschem* **2017**, *10*, 1892–1897; f) P. Zhou, L. Jiang, *Science Advances* **2017**, *3*, e1601945.

[6] a) D. Cantillo, M. M. Moghaddam, C. O. Kappe, *J. Org. Chem.* **2013**, *78*, 4530–4542; b) B. Pieber, D. P. Cox, C. O. Kappe, *Org. Process Res. Dev.* **2016**, *20*, 376–385; c) P. Zhou, C. Yu, L. Jiang, K. Lv, Z. Zhang, *J. Catal.* **2017**, *352*, 264–273.

[7] T. Aditya, A. Pal, T. Pal, *Chem. Commun.* **2015**, *51*, 9410–9431.

[8] P. L. Gkizis, M. Stratakis, I. N. Lykakis, *Catal. Commun.* **2013**, *36*, 48–51.

[9] J. Hu, Y. Ding, H. Zhang, P. Wu, X. Li, *RSC Adv.* **2016**, *6*, 3235–3242.

[10] F. Li, B. Frett, H. Y. Li, *Synlett* **2014**, *25*, 1403–1408.

[11] a) N. R. Guha, D. Bhattacherjee, P. Das, *Tetrahedron Lett.* **2014**, *55*, 2912–2916; b) P. Luo, K. Xu, R. Zhang, L. Huang, J. Wang, W. Xing, J. Huang, *Catal. Sci. Technol.* **2012**, *2*, 301–304.

[12] a) D. Cantillo, M. Baghbanzadeh, C. O. Kappe, *Angew. Chem. Int. Ed.* **2012**, *51*, 10190–10193; b) U. Sharma, P. K. Verma, N. Kumar, V. Kumar, M. Bala, B. Singh, *Chem. - Eur. J.* **2011**, *17*, 5903–5907; c) K. Zhu, M. P. Shaver, S. P. Thomas, *Chem. Sci.* **2016**, *7*, 3031–3035.

[13] a) M. Benz, R. Prins, *Appl. Catal., A* **1999**, *183*, 325–333; b) M. Lauwiner, R. Roth, P. Rys, *Appl. Catal., A* **1999**, *177*, 9–14; c) M. Lauwiner, P. Rys, J. Wissmann, *Appl. Catal., A* **1998**, *172*, 141–148.

[14] a) M. Tian, X. Cui, M. Yuan, J. Yang, J. Ma, Z. Dong, *Green Chem.* **2017**, *19*, 1548–1554; b) M. Tian, X. Cui, K. Liang, J. Ma, Z. Dong, *Inorg. Chem. Front.* **2016**, *3*, 1332–1340.

[15] a) H. B. Sun, Y. J. Ai, D. Li, Z. K. Tang, Z. X. Shao, Q. L. Liang, *Chem. Eng. J.* **2017**, *314*, 328–335; b) Q. Shi, R. Lu, K. Jin, Z. Zhang, D. Zhao, *Green Chem.* **2006**, *8*, 868–870; c) B. Yang, Q. K. Zhang, X. Y. Ma, J. Q. Kang, J. M. Shi, B. Tang, *Nano Res.* **2016**, *9*, 1879–1890.

[16] a) P. S. Kumbhar, J. Sanchez-Valente, J. M. M. Millet, F. Figueras, *J. Catal.* **2000**, *191*, 467–473; b) P. S. Kumbhar, J. Sanchez-Valente, F. Figueras, *Tetrahedron Lett.* **1998**, *39*, 2573–2574; c) Q. Shi, R. Lu, L. Lu, X. Fu, D. Zhao, *Adv. Synth. Catal.* **2007**, *349*, 1877–1881; d) J. R. Chiou, B. H. Lai, K. C. Hsu, D. H. Chen, *J. Hazard. Mater.* **2013**, *248*, 394–400.

[17] a) D. Sarkar, G. G. Khan, A. K. Singh, K. Mandal, *J. Phys. Chem. C* **2012**, *116*, 23540–23546; b) H. Chen, X. Huang, L.-J. Zhou, G.-D. Li, M. Fan, X. Zou, *ChemCatChem* **2016**, *8*, 992–1000.

[18] a) D. W. Kim, I. S. Hwang, S. J. Kwon, H. Y. Kang, K. S. Park, Y. J. Choi, K. J. Choi, J. G. Park, *Nano Lett.* **2007**, *7*, 3041–3045; b) K. Kravchyk, L. Protesescu, M. I. Bodnarchuk, F. Krumeich, M. Yarema, M. Walter, C. Guntlin, M. V. Kovalenko, *J. Am. Chem. Soc.* **2013**, *135*, 4199–4202.

[19] a) B. Wang, L. F. Zhu, Y. H. Yang, N. S. Xu, G. W. Yang, *J. Phys. Chem. C* **2008**, *112*, 6643–6647; b) E. R. Leite, I. T. Weber, E. Longo, J. A. Varela, *Adv. Mater.* **2000**, *12*, 965.

[20] a) K. Vinodgopal, I. Bedja, P. V. Kamat, *Chem. Mater.* **1996**, *8*, 2180–2187; b) J. B. Jiang, J. R. Swierk, K. L. Materna, S. Hedstrom, S. H. Lee, R. H. Crabtree, C. A. Schmuttenmaer, V. S. Batista, G. W. Brudvig, *J. Phys. Chem. C* **2016**, *120*, 28971–28982.
[21] Y. T. Han, X. Wu, Y. L. Ma, L. H. Gong, F. Y. Qu, H. J. Fan, *CrystEngComm* **2011**, *13*, 3506–3510.
[22] a) M. T. Niu, F. Huang, L. F. Cui, P. Huang, Y. L. Yu, Y. S. Wang, *Acs Nano* **2010**, *4*, 681–688; b) P. Sun, X. Zhou, C. Wang, K. Shimanoe, G. Lu, N. Yamazoe, *J. Mater. Chem. A* **2014**, *2*, 1302–1308; c) S. Jana, A. Mondal, *ACS Appl. Mater. Interfaces* **2014**, *6*, 15832–15840.
[23] R. V. Jagadeesh, G. Wienhoefer, F. A. Westerhaus, A.-E. Surkus, M.-M. Pohl, H. Junge, K. Junge, M. Beller, *Chem. Commun.* **2011**, *47*, 10972–10974.
[24] M. T. Zheng, Y. L. Liu, Y. Xiao, Y. Zhu, Q. Guan, D. S. Yuan, J. X. Zhang, *J. Phys. Chem. C* **2009**, *113*, 8455–8459.
[25] K. L. Ai, Y. L. Liu, C. P. Ruan, L. H. Lu, G. Q. Lu, *Adv. Mater.* **2013**, *25*, 998–1003.
[26] N. P. Wickramaratne, M. Jaroniec, *ACS Appl. Mater. Interfaces* **2013**, *5*, 1849–1855.
[27] L. M. Guo, X. Z. Cui, Y. S. Li, Q. J. He, L. X. Zhang, W. B. Bu, J. L. Shi, *Chem. - Asian J.* **2009**, *4*, 1480–1485.
[28] H. W. Bai, Z. Y. Liu, D. D. Sun, *J. Mater. Chem.* **2012**, *22*, 18801–18807.
[29] Y.-M. Lu, H.-Z. Zhu, W.-G. Li, B. Hu, S.-H. Yu, *J. Mater. Chem. A* **2013**, *1*, 3783–3788.
[30] N. P. Wickramaratne, M. Jaroniec, *Chem. Commun.* **2014**, *50*, 12341–12343.
[31] L. R. Kong, X. F. Lu, X. J. Bian, W. J. Zhang, C. Wang, *ACS Appl. Mater. Interfaces* **2011**, *3*, 35–42.
[32] B. Hu, Y. Zhao, H.-Z. Zhu, S.-H. Yu, *Acs Nano* **2011**, *5*, 3166–3171.
[33] a) H. L. Fei, Z. W. Peng, L. Li, Y. Yang, W. Lu, E. L. G. Samuel, X. J. Fan, J. M. Tour, *Nano Res.* **2014**, *7*, 502–510; b) H. W. Zhang, L. Zhou, X. D. Huang, H. Song, C. Z. Yu, *Nano Res.* **2016**, *9*, 3725–3734.
[34] M.-M. Titirici, M. Antonietti, *Chem. Soc. Rev.* **2010**, *39*, 103–116.
[35] a) C. Zhang, J. Lu, M. Li, Y. Wang, Z. Zhang, H. Chen, F. Wang, *Green Chem.* **2016**, *18*, 2435–2442; b) O. Beswick, I. Yuranov, D. T. L. Alexander, L. Kiwi-Minsker, *Catal. Today* **2015**, *249*, 45–51; c) T. Sheng, Y.-J. Qi, X. Lin, P. Hu, S.-G. Sun, W.-F. Lin, *Chem. Eng. J.* **2016**, *293*, 337–344.
[36] P. S. Rathore, R. Patidar, T. Shripathi, S. Thakore, *Catal. Sci. Technol.* **2015**, *5*, 286–295.
[37] a) L. J. Ren, G. N. Zhang, Z. Yan, L. P. Kang, H. Xu, F. Shi, Z. B. Lei, Z. H. Liu, *Electrochim. Acta* **2017**, *231*, 705–712; b) T. T. Liu, Y. H. Zhu, E. H. Liu, Z. Y. Luo, T. T. Hu, Z. P. Li, R. Ding, *Trans. Nonferrous Met. Soc. China* **2015**, *25*, 2661–2665.

Submitted: July 26, 2017
Revised: September 5, 2017
Accepted: September 6, 2017